Journal of Power Sources 245 (2014) 947–952

Contents lists available at SciVerse ScienceDirect

Journal of Power Sources

journal homepage: www.elsevier.com/locate/jpowsour

Short communication

Stability of carbon electrodes for aqueous lithium-air secondary batteries

Hirokazu Ohkuma, Ichiro Uechi, Masaki Matsui, Yasuo Takeda, Osamu Yamamoto*, Nobuyuki Imanishi

Graduate School of Engineering, Mie University, 1577 Kurimamachiya-cho, Tsu, Mie 514-8507, Japan

HIGHLIGHTS

- Air electrodes of carbon materials were examined in saturated LiOH with 10 M LiCl.
- The lowest over-potential was observed for Ketjen black.
- CO was detected after polarization for the oxygen evolution reaction.

ARTICLE INFO

Article history:
Received 23 April 2013
Received in revised form
30 May 2013
Accepted 26 June 2013
Available online 16 July 2013

Keywords:
Aqueous lithium-air battery
Oxygen electrode
Carbon electrode
High energy density battery

ABSTRACT

The air electrode performance of various carbon materials, such as Ketjen black (KB), acetylene black (AB and AB-S), Vulcan XC-72R (VX), and vapor grown carbon fiber (VGCF) with and without $La_{0.6}Sr_{0.4}Co_{0.2}Fe_{0.8}O_3$ (LSCF) catalyst were examined in an aqueous solution of saturated LiOH with 10 M LiCl in the current density range 0.2–2.0 mA cm^{-2}. The best performance for oxygen reduction and evolution reactions was observed for the KB electrode, which has the highest surface area among the carbon materials examined. A steady over-potential of 0.2 V was obtained for the oxygen reduction reaction using the KB electrode without the catalyst, while the over-potential was 0.15 V for KB with the LSCF catalyst at 2.0 mA cm^{-2}. The over-potentials for the oxygen evolution reaction were slightly higher than those for the oxygen reduction reaction, and gradually increased with the polarization period. Analysis of the gas in the cell after polarization above 0.4 V revealed the evolution of a small amount of CO during the oxygen evolution reaction by the decomposition of carbon in the electrode. The amount of CO evolved was significantly decreased by the addition of LSCF to the carbon electrode.

1. Introduction

Lithium-air secondary batteries consist of lithium metal as the anode active material and oxygen as the cathode active material have high potential for electric vehicle applications because they have an extremely high theoretical energy density. The rechargeable lithium–oxygen battery was first reported in 1996 by Abraham and Jiang [1], which was comprised of a lithium ion conductive gel-type polymer electrolyte, a lithium metal anode, and a carbon electrode with cobalt phthalocyanine as the catalyst. Kuboki et al. [2] reported an extremely high discharge capacity of 5360 mAh g^{-1} (based on carbon mass) for a primary lithium-air cell with a hydrophobic ionic liquid electrolyte. Bruce et al. [3,4] presented more attractive results for a rechargeable lithium-oxygen cell using an organic electrolyte of 1 M $LiPF_6$ in propylene carbonate and a carbon black air electrode with a MnO_2 catalyst, in which a high charge and discharge capacity of 600 mAh g^{-1} (based on carbon mass) was achieved after 50 cycles. More recently, Scrosati and colleagues [5] reported a lithium-oxygen rechargeable battery that consisted of a tetra (ethylene) glycol dimethyl ether-$LiCF_3SO_3$ electrolyte and an air electrode with Super P carbon and carbon paper, which was operated over 30 cycles with a high capacity of 5000 mAh g^{-1} (based on carbon mass). However, such rechargeable lithium–oxygen batteries with non-aqueous electrolytes have many problems that must be addressed, such as the reaction of the electrolyte and lithium with water from the atmosphere, lithium dendrite formation on the lithium electrode during the charge process, and high polarization during the charge and discharge processes.

* Corresponding author. Tel.: +81 59 231 9420.
E-mail addresses: Yamamoto@chem.mie-u.ac.jp, osyamamo@alles.or.jp (O. Yamamoto).

0378-7753
http://dx.doi.org/10.1016/j.jpowsour.2013.06.146

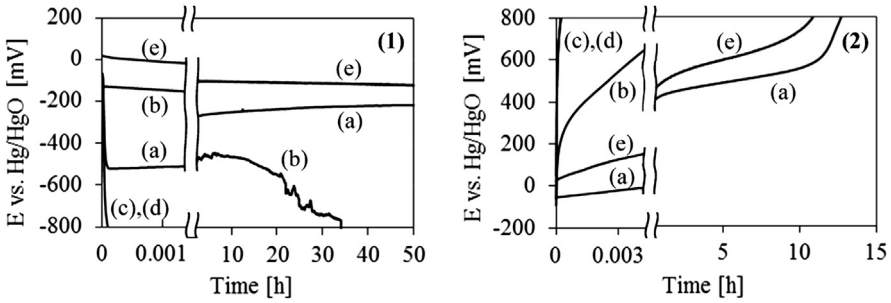

Fig. 1. Electrode potentials *vs.* time at 0.5 mA cm^{-2} for (1) ORR and (2) OER with (a) KB, (b) Vx, (c) VGCF, (d) AB, and (e) AB-S at room temperature.

Some of the problems observed in non-aqueous systems could be removed by employing an aqueous system. An aqueous lithium-air battery system could be constructed using a water-stable lithium-conducting solid electrolyte of $Li_{1+x}Al_xTi_{2-x}(PO_4)_3$ (LATP) as a protective layer between the lithium metal anode and aqueous electrolyte [6–10]. The reaction mechanism for aqueous lithium-air batteries is different from that for non-aqueous lithium-air batteries. In the case of the aqueous system, the cell reaction is:

$$4Li + O_2 + 6H_2O \rightleftarrows 4LiOH \cdot H_2O. \quad (1)$$

The discharge product of $LiOH \cdot H_2O$ is soluble in the aqueous electrolyte. For the aqueous system, water molecules are involved in the redox reaction at the air cathode and the theoretical energy density of 1910 Wh kg^{-1} is lower than that for the non-aqueous system at 3457 Wh kg^{-1}. We have previously reported the oxygen reduction reaction (ORR) and oxygen evolution reaction (OER) in an aqueous solution of saturated LiOH with 10 M LiCl at a carbon air electrode with various perovskite-type oxides as the catalyst component [11]. The aqueous electrolyte of saturated LiOH with 10 M LiCl was used for the stability of LATP, because LATP is unstable in saturated LiOH aqueous solution [9], but is stable in saturated LiOH with 10 M LiCl [12]. The over-potentials for the ORR and OER in saturated LiOH with 10 M LiCl were considerably lower than those in the non-aqueous electrolyte. However, the long term stability of the carbon air electrode was not examined in the previous study. In this study, we examine the long term performance of various types of carbon electrodes with and without $La_{0.6}Sr_{0.4}Co_{0.2}Fe_{0.8}O_3$ (LSCF) as a catalyst for the ORR and OER in the aqueous electrolyte of saturated LiOH with 10 M LiCl.

2. Experimental

The perovskite-type oxide $La_{0.6}Sr_{0.4}Co_{0.2}Fe_{0.8}O_3$ (LSCF) was purchased from Seimi Chemical Co. The specific surface area was measured to be 1.79 $m^2\ g^{-1}$. Ketjen Black EC-600JD (KB; Lion Co.), acetylene carbon black (AB; Strem Chemicals), high surface area acetylene carbon black (AB-S), Vulcan XC-72R (VX; Cabot Co.), and vapor grown carbon fiber (VGCF; Showa Denko) were used for the air electrodes.

The air electrodes consisted of a reaction layer and an air diffusion layer. The reaction layer was prepared by mixing the carbon substrate, LSCF, and polytetrafluoroethylene (PTFE) in water with a surfactant of poly(oxyethelene)-octylphenyl ether using ultrasonication. The weight ratio of carbon:LSCF:PTFE was 55:30:15, and the carbon:PTFE ratio was 85:15 for the electrode without LSCF. The mixture was dried at 90 °C and heated at 280 °C to fix the PTFE onto a Ti mesh (100 mesh) with the diffusion layer under pressure at 64 MPa. The air diffusion layer was prepared by mixing AB and PTFE (7:3 weight ratio). The air electrodes were tested in an aqueous solution of saturated LiOH with 10 M LiCl. The test cell was a beaker cell equipped with a working electrode (active area of 0.64 cm^2), a platinum plate with platinum black as a counter electrode, and a Hg/HgO or platinum plate/platinum black reference electrode. Experiments were conducted at room temperature and under a CO_2-free air atmosphere. The electrode potentials were measured using a potentiostat/galvanostat (Hokuto Denko, HJ-1001SD8) and the electrode impedance was measured using a multichannel potentiostat/galvanostat (Biologic VMP 3). The gas evolved under the ORR and OER was analyzed using a gas chromatograph (GL Science, GC-3200). The working electrode, platinum counter electrode, and Hg/HgO reference electrode were set in a closed cell with a small hole for gas collection.

The surface area and pore distribution of the carbon materials were measured using a gas adsorption analyzer (Shimadzu Co., Tristar 3000). The contact angles of the carbons were measured using a contact angle meter (Kyowa Interface Science DMs-400), where the aqueous solution of saturated LiOH with 10 M LiCl was dropped on the surface of carbon pellets.

3. Results and discussion

Fig. 1 shows the changes in electrode potential with polarization period at 0.5 mA cm^{-2} for the various carbon materials without the LSCF catalyst, where the thickness of the reaction layer and gas diffusion layer were both approximately 0.2 mm. The over-potentials for the ORR on AB and VGCF quickly decreased with the polarization period. The current densities at −0.4 V *vs.* Hg/HgO for the AB and VGCF electrodes were 0.04 and 0.12 mA cm^{-2}, respectively. In contrast, the KB, AB-S, and VX electrodes exhibited more steady polarization behavior and the current densities at −0.4 V *vs.* Hg/HgO were 11.9, 13.2, and 0.26 mA cm^{-2}, respectively. The KB and AB-S electrode have a steady electrode potential for 50 h, whereas that for the VX electrode decreased gradually with the polarization period. The AB and VGCF electrodes, as well as the VX electrode, had high over-potentials for the OER, but the KB and AB-S electrode showed a steady potential for approximately 10 h after which the potential increased significantly with the polarization period. The physical properties of these carbon materials

Table 1
Current densities at −0.4 V *vs.* Hg/HgO for ORR (I_R) and at 0.6 V *vs.* Hg/HgO for OER (I_E) and physical properties of the carbon materials.

	KB	AB-S	VX	AB	VGCF
I_R at −0.4 V vs. Hg/HgO (mA cm^{-2})	11.9	13.2	0.26	0.04	0.12
I_E at 0.6 V vs. Hg/HgO (mA cm^{-2})	22.6	12.6	0.12	0.06	0.10
Surface area ($m^2\ g^{-1}$)	1292	829	215	87	13
Pore volume (mL g^{-1})	1.36		0.64	0.41	0.06
Crystallite[a] (I_D/I_G)	1.128	2.00	0.813	1.25	0.065
Contact angle (°)[b]	128	121	48	108	135

[a] Intensity ratios of D and G bands in Raman spectra from Refs. [13] and [14].
[b] Measured using aqueous solution of saturated LiOH with 10 M LiCl.

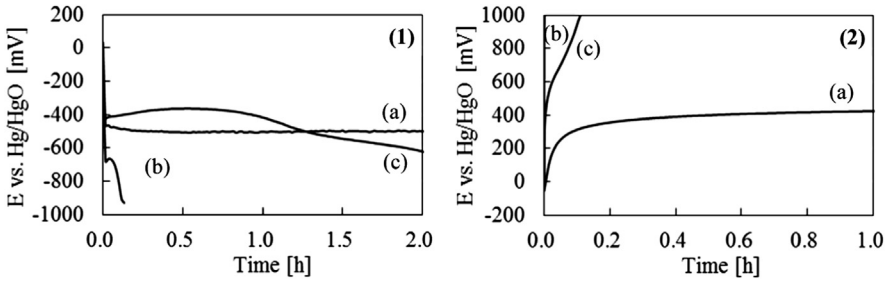

Fig. 2. Electrode potentials *vs.* polarization period at 5 mA cm^{-2} for (1) ORR and at 1.0 m cm^{-2} and for (2) OER with (a) KB, (b) VX, and (c) KB and VX (1:1 weigh ratio).

and the current densities for the ORR at −0.4 V *vs.* Hg/HgO and those for the OER at 0.6 V *vs.* Hg/HgO are summarized in Table 1; the specific surface areas and contact angles were measured in this study and the crystallite data were taken from Refs. [13] and [14]. The over-potentials for the ORR and OER are significantly dependent on the specific surface areas of the carbon materials. The highest current density at −0.4 V *vs.* Hg/HgO for the ORR was observed for the AB-S electrode and that at 0.6 V vs. Hg/HgO for the OER was observed for the KB electrode. These carbons have the high specific surface area. The VGCF and AB electrodes, which have the low specific surface areas, showed a low current density at −0.4 and 0.6 V *vs.* Hg/HgO. The polarization behaviors of KB, VX, and the mixture of KB and VX (1:1 w/w) were examined at high current densities. Fig. 2 shows the results for the ORR at 5 mA cm^{-2} and for the OER at 1.0 mA cm^{-2}. The mixed electrode of KB and VX had low over-potentials for the ORR, but high over-potentials for the OER. The high crystalline carbon of VX may prevent the OER. The effect of the air diffusion electrode thickness on the over-potentials for the ORR and OER was examined. The thickness of the diffusion layer had no effect on the polarization in the range of 0.1–0.5 mm for current densities up to 2.0 mA cm^{-2}. However, the over-potentials for the ORR and OER at higher current densities were affected by the thickness of the reaction layer; the over-potential decreased with increasing electrode thickness. This may be due to an increase of the active reaction area with increasing thickness. Fig. 3 shows plots of potential for the ORR and OER *vs.* the current density per weight of KB for various reaction layer (RL) thicknesses, where the area current densities were 2.0 and 0.2 mA cm^{-2}. The plots show one line as a function of the thickness of the electrode at different current densities *per* surface area. If the electrolyte is penetrated homogeneously into the KB and PTFE composite electrode, the contact surface area of KB with the electrolyte is proportional to the weight of KB. These plots suggest that the over-potential is dependent on the contact surface area of carbon with the electrolyte, where oxygen in the electrolyte reacts with water to produce OH^- (or HO_2^-) (ORR) and OH^- is oxidized to O_2 (OER). The high over-potential on VGCF and AB could be explained by their low surface areas. The effects of the crystallite features and the contact angle of the carbon on ORR and OER are not clear at present. The over-potentials for the ORR at 75 and 500 mA g-carbon^{-1} were 0.15 and 0.25 V, respectively and the over-potential for the OER at 75 and 500 mA g-carbon^{-1} 0.39 and 0.59 V, respectively, which are compared with those of 0.25 V for the ORR and 1.2 V for the OER at 75 mA g-carbon^{-1} on an electrode of Super P carbon with a catalyst in a non-aqueous electrolyte [4]. The over-potential for the OER in the non-aqueous electrolyte is much higher than that in the aqueous electrolyte. The difference may be due to the resistance of

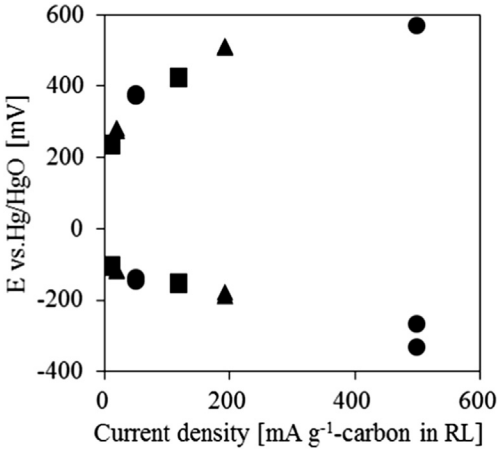

Fig. 3. Electrode potentials *vs.* current density per gram of KB. Reaction layer thickness: ●, 0.10 mm; ▲, 0.20 mm; ■: 0.30 mm.

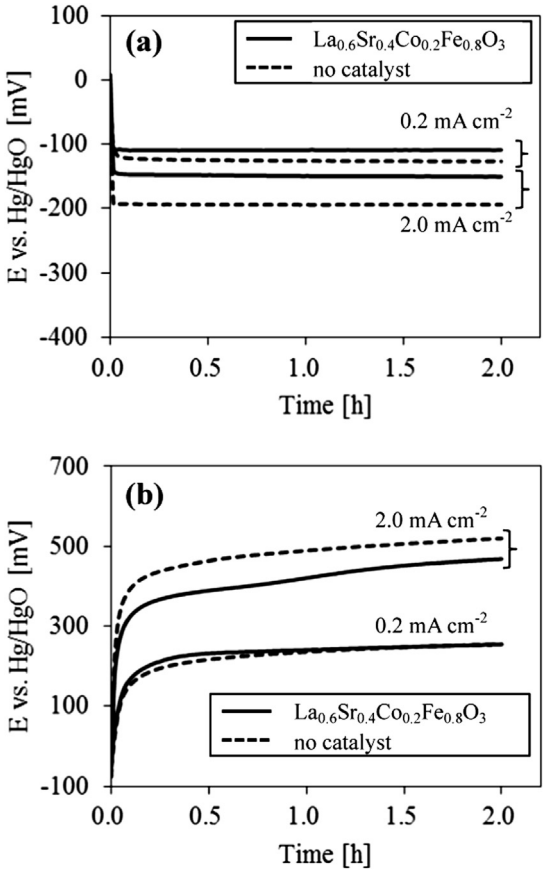

Fig. 4. Electrode potential *vs.* polarization period at 0.2 and 2.0 mA cm^{-2} for the (a) ORR and (b) OER using KB electrodes with and without LSCF.

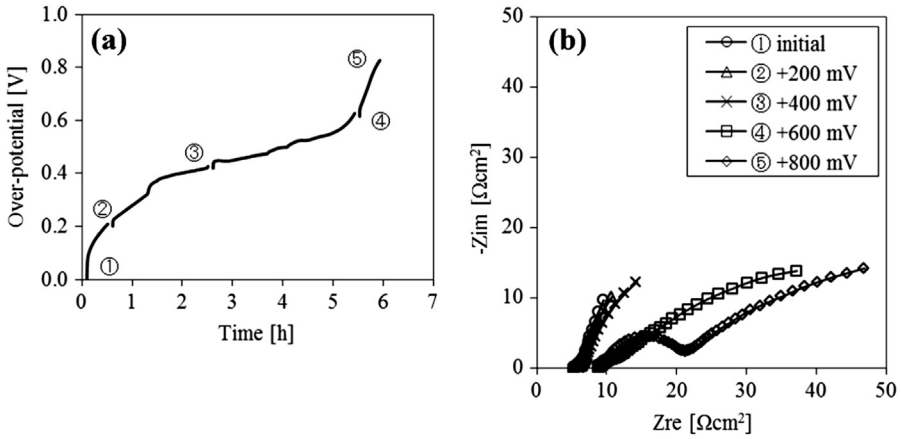

Fig. 5. (a) Change in over-potential with time for the OER with the KB electrode at 1 mA cm^{-2} and (b) impedance profiles for each stage shown in Fig. 5-(a).

Li_2O_2 to electrochemical oxidation compared to that of OH^-. We have previously reported [11] that the LSCF perovskite-type oxide has catalytic activity for the ORR and OER in an aqueous solution of saturated LiOH with 10 M LiCl. In this study, the effect of this catalyst on the ORR and OER were examined for a longer period. Fig. 4 compares the change in electrode potential over polarization periods at 0. 2 and 2.0 mA cm^{-2} for KB electrodes with and without LSCF, where the thickness of the reaction layer was approximately 0.3 mm and the LSCF content was 30 wt%. The addition of LSCF into the KB electrode improved the over-potentials for the ORR and OER, especially at the higher current density of 2.0 mA cm^{-2}. The KB electrode with LSCF had a steady over-potential of 0.15 V for 2 h for the ORR, while the over-potentials at 2.0 mA cm^{-2} for the OER increased gradually to 0.5 V after 2 h. A steady over-potential of 0.2 V was observed at a low current density of 0.2 mA cm^{-2}.

To confirm the degradation process for the OER, the electrode impedance was measured as a function of the polarization time at 1 mA cm^{-2}. Fig. 5 shows the change in over-potential at 1 mA cm^{-2} with the polarization period and the impedance change of the KB electrode without LSCF at each stage of the polarization period for the OER (charging process in the lithium-air cell); the electrode potential and impedance of the air electrode were measured using the platinum/platinum black reference electrode. No significant change in electrode impedance was observed in the plateau potential range, where a small semicircle followed by a straight line was observed. The frequency of the top of the semicircle was 10^2 Hz. However, when the electrode was polarized for longer periods, the electrode potential increased significantly, and a large semicircle was observed in the same frequency range. The intercept of the semicircle with the real axis at a high frequency increased with increase in the polarization period, which indicates an increase in electrolyte resistance. The increase in the electrolyte resistance may be due to the accumulation of oxygen gas on the carbon surface, which results in a decrease of the contact area between the electrolyte and carbon surface. The origin of the large semicircle unclear, but one possibility may be the high charge transfer resistance for the OER, which could be caused by a change in the catalytic activity of the carbon surface for the OER. The decrease in the catalytic activity of the carbon surface may be explained by electrochemical reaction of the carbon electrode with oxygen, as discussed later. The electrode polarized for 6 h was switched to the ORR (discharge process in the lithium-air cell) and polarized at 1.0 mA cm^{-2} for 6 h. The electrode impedance was then measured at each stage. The change in over-potential at 1 mA cm^{-2} with the polarization time and the impedance profiles at each stage are shown in Fig. 6-(a) and (b), respectively. The electrolyte resistances at each stage were almost the same as that of the electrode anodically polarized for 6 h shown in Fig. 5-(b). The large semicircles were observed at every stage after cathodic polarization and the diameters of the semicircles are almost same.

Shimizu et al. [15] reported the over-potential for ORR and OER on a carbon black (surface area of 830 $m^2\ g^{-1}$) with a $La_{0.6}Ca_{0.4}CoO_3$

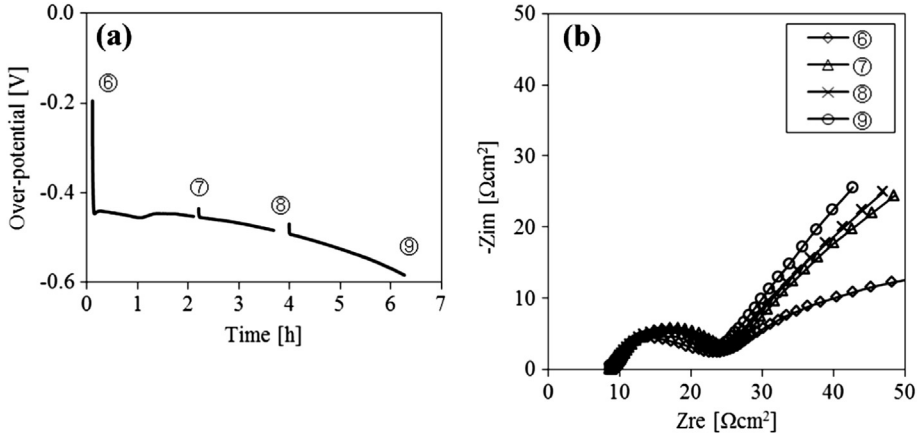

Fig. 6. (a) Change in over-potential with time for the ORR with the KB electrode at 1 mA cm^{-2} and (b) impedance profiles for each stage shown in Fig. 6-(a).

catalyst in a 7 M KOH solution and found a electrode potential of −125 mV vs. Hg/HgO at a current of 130 mA cm^{-2} for the carbon black electrode without the catalyst. The electrode with the catalyst was stable for 100 cycles of charge and discharge test at a current density of 100 mA cm^{-2}. The stability of the electrode without the catalyst was not reported. Arai et al. [16] examined the KB electrode (surface area of 1300 m^2 g^{-1}) for the ORR and OER in aqueous 8 M KOH solution and found an electrode potential of −180 mV *vs.* Hg/HgO at 100 mA cm^{-2} for ORR and 500 mV *vs.* Hg/HgO at 50 mA cm^{-2} for OER. The over-potentials for ORR and OER in the saturated LiOH with 10 M LiCl aqueous solution are higher than those in the high concentration of KOH solution. Arai et al. also observed electrode deterioration during the OER and claimed that the degradation resulted in a loss of the electrochemically active surface area of the electrode, mainly due to carbon corrosion. However, the carbon corrosion was not directly measured during the OER. More recently, Bruce et al. [17] also reported that carbon is unstable upon charging above 3.5 V vs. Li/Li^+ in a non-aqueous electrolyte, and upon discharge, there is little or no decomposition if the carbon is hydrophobic, whereas some decomposition does occur for hydrophilic carbon. In this study, the gas in the cells with the KB, VX, and AB-S electrodes was analyzed after polarization for 10 h as a function of the electrode potential. For all these three of these carbon electrodes, hydrogen and CO were observed for the OER and not observed for the ORR, where the amount molar ratio of hydrogen to CO was approximately 10. The hydrogen gas was produced on the platinum counter electrode by the cathodic reaction of H^+ in the electrolyte, the amount of which was approximately 0.1% of that calculated from the coulombs passed through the cell. The CO gas may come from the carbon electrode, because there was no carbon source in this cell, except the carbon in the electrode. We could not observe CO_2, because the aqueous solution of saturated LiOH with 10 M LiCl (pH ~8) dissolves CO_2. Fig. 7 shows the relationship between the over-potential and percentage of produced CO to the amount calculated from the coulombs passed through the cell, assuming the following reaction:

$$C + 2OH^- = CO + H_2O + 2e. \quad (2)$$

The percentage of CO increased linearly with the electrode potential for the KB, AB-S and VX electrodes. A high current could not be passed through the cells with the VGCF and AB electrodes, so that gas evolution could not be evaluated. However, as Bruce et al. reported (16), the hydrophobic carbons (KB and AB-S), which show high contact angle with aqueous electrolytes, produce less CO than the hydrophilic carbon (VX). The high over-potentials of the mixed electrode of KB and VX for OER shown in Fig. 2 could be explained by the easy electrochemical decomposition of VX. At lower electrode over-potential, such as 300 mV *vs.* OCV, no CO gas and a small amount of hydrogen was observed, which suggests that the carbon electrode may be electrochemically oxidized during the OER at above 300 mV *vs.* OCV. Fig. 8 shows the percentage of CO *vs.* over-potential for the KB electrode with LSCF as a function of the LSCF content. The percentage of CO was significantly decreased by the addition of 30 wt% LSCF, although a small amount of CO was still observed. The electrode potential increase with increasing polarization period at 2.0 mA cm^{-2} shown in Fig. 4 could be explained by electrochemical oxidation of the KB surface, which would result in a deterioration of the catalytic activity of KB for the OER. The oxidation of carbon is a serious problem for the long term stability of the air electrode; therefore, a more stable catalyst for the ORR and OER, especially for the OER, should be developed for the air electrode with a lower over-potential at a high current density.

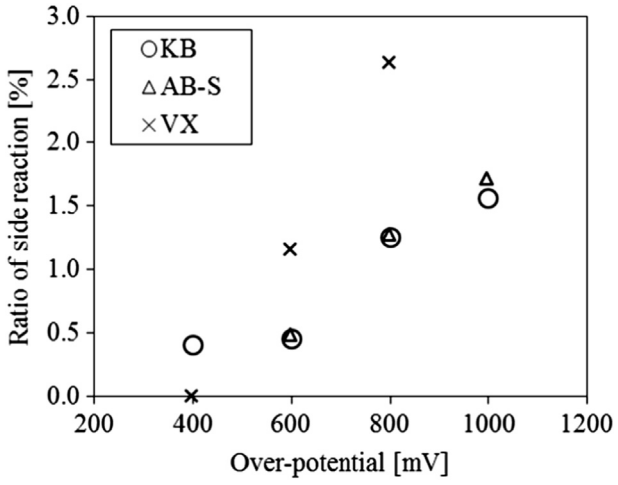

Fig. 7. Relationship between the over-potential and percentage of CO produced to the weight calculated from the coulombs passed through the Pt, air/saturated LiOH with 10 M LiCl aqueous solution/KB (or VX, AB-S), air cell.

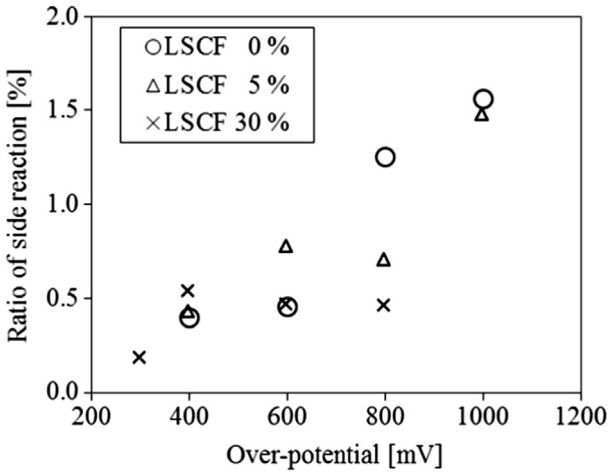

Fig. 8. Relationship between the over-potential and percentage of CO produced to the weight calculated from the coulombs passed through the Pt, air/saturated LiOH with 10 M LiCl aqueous solution/KB with LSCF, air cell.

4. Conclusions

The behavior of the various carbon air electrodes in a Li-air cell with an aqueous electrolyte of saturated LiOH with 10 M LiCl was examined. Carbon with a high surface area, such as Ketjen black, exhibited stable electrode potentials for the ORR over a long polarization period at 2.0 mA cm^{-2}; however, the electrode potentials for the OER increased with the polarization period. The gases evolved during the OER were analyzed and confirmed to be CO and H_2. Degradation of the electrode performance during the OER could be explained by corrosion of the carbon surface, which resulted in a loss of catalytic activity for the OER. The electrode performance of the carbon electrode for OER was improved and the amount of CO was significantly decreased by the addition of LSCF catalyst.

Acknowledgments

This study was supported by the Japan Science and Technology Agency (JST) under the project “Advanced low Carbon Technology Research and Development program”.

References

[1] K.M. Abraham, Z. Jiang, J. Electrochem. Soc. 143 (1996) 1.
[2] T. Kuboki, T. Okuyama, T. Ohsaki, N. Takami, J. Power Sources 146 (2005) 766.
[3] T. Ogasawara, A. Debart, M. Holzapfel, P.G. Bruce, J. Am. Chem. Soc. 128 (2006) 1390.
[4] A. Debart, A.J. Paterson, J. Bao, P.G. Bruce, Angew. Chem. Int. Ed. 47 (2008) 4521.
[5] H.G. Jung, J. Hassoun, J.B. Park, Y.K. Sun, B. Scrosati, Nat. Chem. 4 (2012) 579.
[6] S.J. Visco, E. Nimon, B. Katz, L.D. Jonghe, M.Y. Chu, 210th ECS Meeting Abstract #389, 2006.
[7] S.J. Visco, E.S. Nimon, L.D. Jonghe, 219th ECS Meeting Abstract #436, 2011.
[8] S.J. Visco, E. Nimon, B. Katz, M.Y. Chu, L.D. Jonghe, PRIME 2012 Abstract #1156, 2012.
[9] N. Imanishi, S. Hasegawa, T. Zhang, A. Hirano, Y. Takeda, O. Yamamoto, J. Power Sources 185 (2008) 1392.
[10] T. Zhang, N. Imanishi, S. Hasegawa, A. Hirano, J. Xie, Y. Takeda, O. Yamamoto, N. Sammes, Electrochem. Solid-State Lett. 12 (2009) A132.
[11] H. Ohkuma, I. Uechi, N. Imanishi, A. Hirano, Y. Takeda, O. Yamamoto, J. Power Sources 223 (2013) 319.
[12] Y. Shimonishi, T. Zhang, N. Imanishi, D. Im, D.J. Lee, A. Hirano, Y. Takeda, O. Yamamoto, N. Sammes, J. Power Sources 196 (2011) 5128.
[13] T. Kim, C. Ham, C.K. Rhee, S.-H. Yoo, M. Tsuji, I. Mashida, Carbon 47 (2009) 226.
[14] S. Nakanishi, F. Mizuno, K. Nobuhara, T. Abe, Carbon 50 (2012) 4794.
[15] Y. Shimizu, K. Uemura, H. Matsuda, N. Miura, N. Yamazoe, J. Electrochem. Soc. 137 (1990) 3430.
[16] H. Arai, S. Muller, O. Haae, J. Electrochem. Soc. 147 (2000) 3584.
[17] M.M.O. Thotiyl, S.A. Freunberger, A. Peng, P.G. Bruce, J. Am. Chem. Soc. 135 (2013) 494.